JOURNAL OF MATERIALS SCIENCE 20 (1985) 1763–1772

Electrical conduction in some important copper based superionic solids

O. P. SRIVASTAVA, A. K. SRIVASTAVA, H. B. LAL
Department of Physics, University of Gorakhpur, Gorakhpur, India

Measurement of the thermoelectric power (S) and electrical conductivity (σ) of six superionic solids namely CuI, $CuPb_3Br_7$, Cu_2HgI_4, Cu_3CdI_5, Cu_3RbCl_4, $Cu_7(C_6H_{12}NH_3)Br_8$ and $Cu_{16}Rb_4I_7Cl_{13}$ are reported from 300 K to nearly the melting point of each material. The $\log \sigma T$ and S against T^{-1} plots are linear in some temperature ranges with different slopes. For each material they show two distinct regions: one corresponding to superionic (SP) and the other to normal phase (NP). In the superionic phase, Cu^+ ions are the main entity of charge carrier and an extended lattice gas model explains the transport mechanism fairly well. On the higher temperature side of SP, the other cation in the material starts contributing significantly to σ. In the normal phase the conduction is mainly due to Frenkel defects (Cu^+ ions at interstitial sites). The enthalpy for migration and heat of transport of these defects has also been evaluated for CuI, $CuPb_3Br_7$, Cu_2HgI_4 and Cu_3CdI_5. The formation energy of defects has also been calculated for CuI and Cu_3CdI_5. Normal phase has not been obtained in Cu_3RbCl_4, $Cu_7(C_6H_{12}NCH_3)Br_8$ and $Cu_{16}Rb_4I_7Cl_{13}$ as their phase transition temperatures lie below room temperature.

1. Introduction

Active research on copper based superionic solids began in 1973. The main reason for this interest has been the cheaper cost of these materials compared to silver based superionic solids, which were discovered, studied and used in various applications since they came into the limelight in 1967. The main drawback of these materials is the oxidation of the mobile copper ion from the Cu^+ state to Cu^{2+} state which introduces electronic conductivity and limits the potential applications of these compounds. In spite of this limitation several such materials have been discovered, investigated and put to some applications during the last ten years [1–14]. Thermoelectric power measurements, which give heat of transport and information regarding conduction mechanisms and decides the suitability of a model to describe the situation of the solid in the superionic phase, have not yet been reported for many of these solids. This paper presents such studies on some selected copper based superionic solids in both normal and superionic phases. The materials investigated are CuI, $CuPb_3Br_7$, Cu_2HgI_4, Cu_3CdI_5, $Cu_3Rb_4Cl_4$, $Cu_7(C_6H_{12}NCH_3)Br_8$ and $Cu_{16}Rb_4I_7Cl_{13}$. Some physical parameters of these materials are given in Table I.

2. Material preparation and experimental techniques

CuI and other base materials such as CuBr, RbCl, $PbBr_2$, HgI_2, CdI_2 etc. with a stated purity of 99.99% were procured from standard firms. All the materials studied were prepared by firing a pellet of the stoichiometric mixture of appropriate base compounds for several hours in an evacuated sealed pyrex tube between 400 to 500 K. The details are described elsewhere [16–18]. At the beginning of this study, Professor Takahashi, of Nagoya University, Japan provided a few grams of $CuPb_3Br_7$ and $Cu_7(C_6H_{12}NCH_3)Br_8$ which we prepared by the method reported elsewhere [16, 17]. The measurements of electrical conductivity (σ) and thermoelectric power (S) were performed on pellets. Details of pellet making, electrode processing and the techniques

0022–2461/85 $03.00 + .12

TABLE I Physico-chemical parameters of the materials studied

Material	Colour	d (10^{-3} kg m^{-3})	T_p (K)	T_m (K)	Reference
CuI	Light brown	6.0	542	878	[2]
$CuPb_3Br_7$	Light blue	6.4	430	573	[6]
Cu_2HgI_4	Reddish brown	5.6	342	–	[14]
Cu_3CdI_5	Dark red	4.8	515	760	[19]
Cu_3RbCl_4	Darkgreen	3.4	–	575	[9]
$Cu_7Q\,Br_8$	Light yellow	4.5	–	–	[1]
$C_{16}Rb_4I_7Cl_{13}$	Green	4.47	248	507	[12]

d, density; T_p, Phase transition temperature; T_m, melting point; $Q = C_6H_{12}N_4CH_3$.

and procedure employed in σ and S measurement were similar to those reported in several publications of our group [16–22].

3. Results

Electrodes play a significant role in the measurement of both σ and S. The stringent criterion [21] is to have ohmic contact in both measurements. Furthermore, in measurement of S, ideally the electrode material should be a metal of the conducting ion species in the superionic solid. This ensures reduction of heterogeneous thermoelectric power which is unwanted in the interpretation of data [20, 21]. Copper is ideally the best electrode for copper based superionic solids, therefore, copper electrodes were preferred for our investigations. Copper forms ohmic contact on the electrolyte phase in a wide range of applied electric field as is evident from the straight line J against E plots shown in Fig. 1 for two of the representative samples. Similar plots are obtained for others. In all measurements, E was kept in the range in which plots of J against E remained linear.

The measurements reported in this paper were performed on pellets (pressed powders). In such

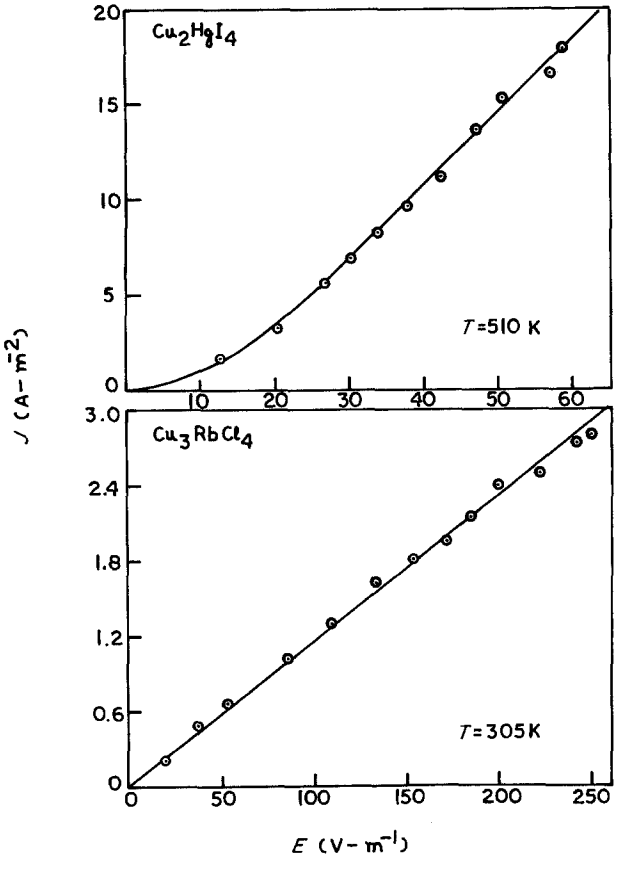

Figure 1 Plots of current density (J) against applied electric field (E) for Cu_2HgI_4 and Cu_3RbCl_4.

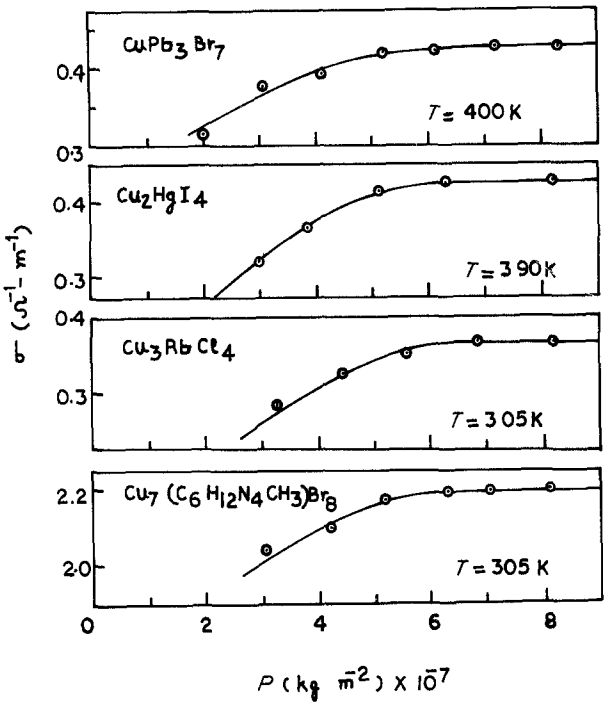

Figure 2 Plots of electrical conductivity (σ) against pelletizing pressure (P) for a few copper based superionic solids.

samples air pores and grain boundaries have a significant effect on the values of electrical conductivity as well as thermoelectric power. Air-pores can be minimized by taking very fine uniform grain powders and making pellets at higher pressure. To see how pores affect the values of σ, measurements of σ as a function of pelletizing pressure were made. The measurements were carried out after the source of pressure had been removed. Fig. 2 shows the results of such measurements. The behaviour in general is similar for all compounds. Electrical conductivity initially increases rapidly with pressure $P = 4 \times 10^7$ kg m^{-2}, then this increase becomes slow and finally tends to become constant when P exceeds 6 to 7×10^7 kg m^{-2}. The densities (Fig. 3) have almost the same type of variation with P. The density of pellets prepared at P exceeding 7×10^7 kg m^{-2} approaches the density of polycrystalline samples*. These results indicate that air pores are significantly reduced for highly pressed pellets and the results on such pellets essentially refer to the material of the pellet. The measurement of σ on highly pressed pellets was carried out at a.c. signal frequencies of 50, 10^2, 10^3 and 10^4 Hz at different temperatures and the results are shown in Fig. 4. σ is practically independent of frequency. This shows that grain boundary effects are not very important in these samples. The majority of superionic solids undergo phase transition from low conducting β-phase to high conducting α-phase. Their physical behaviour is such that the low temperature phase may be referred to as the normal phase (NP) and the high temperature phase as the superionic phase (SP). We have been able to see the behaviour of σ around the phase transition temperature (T_p) for solids in which it is above room temperature. All show a typical hysteresis around T_p. However values of σ remain the same 5 to 10 K above and below the phase transition temperature. Typical plots of $\log \sigma T$ against T^{-1} and S against T^{-1} for the materials studied are given in Figs. 5 and 6. These plots are linear in some temperature range or the other. Thus they can be represented in the form of the equations

$$S = -\frac{Q}{eT} + H \qquad (1)$$

and

$$T\sigma = C \exp\left(-\frac{E_a}{kT}\right) \qquad (2)$$

where Q, H, C and E_a are constants for the material in the different ranges of temperature and e, and k are the magnitudes of electronic charge and the

*Solid samples obtained after melting and slowly cooling it. This type of sample has not been used for investigation because of possible Cu^{2+} contamination on heating.

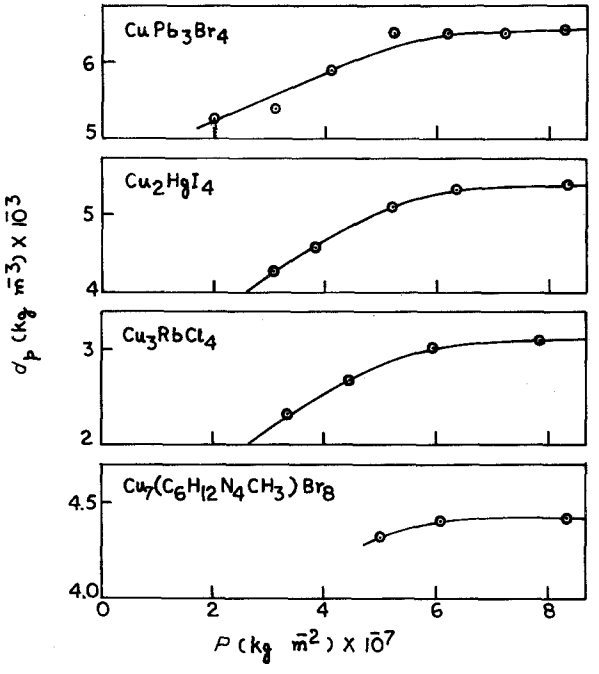

Figure 3 Plots of density (d) against pelletizing pressure (P) for a few copper based superionic solids.

Boltzmann constant, respectively. The summarized results for thermoelectric power which includes the values of Q and H and its temperature range, are given in Table II, and the results of electrical conductivity which includes the value of C, E_a and its range are given in Table III.

4. Discussion

As mentioned earlier, the compounds studied in this paper are not synthesized for the first time but some have been reported and studied by earlier workers. The most common study is that of electrical conductivity. In some cases thermoelectric

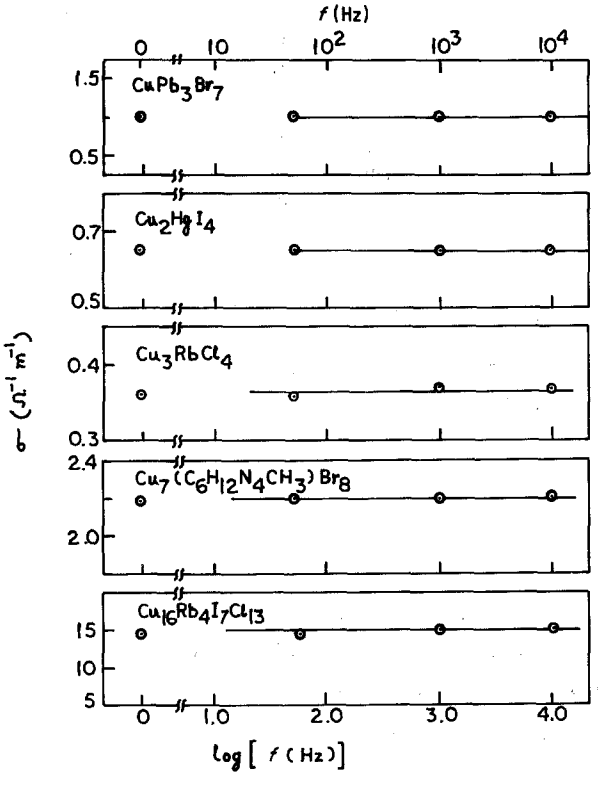

Figure 4 Plots of electrical conductivity (σ) against applied a.c. signal frequency (f) for a few of the copper based superionic solids studied.

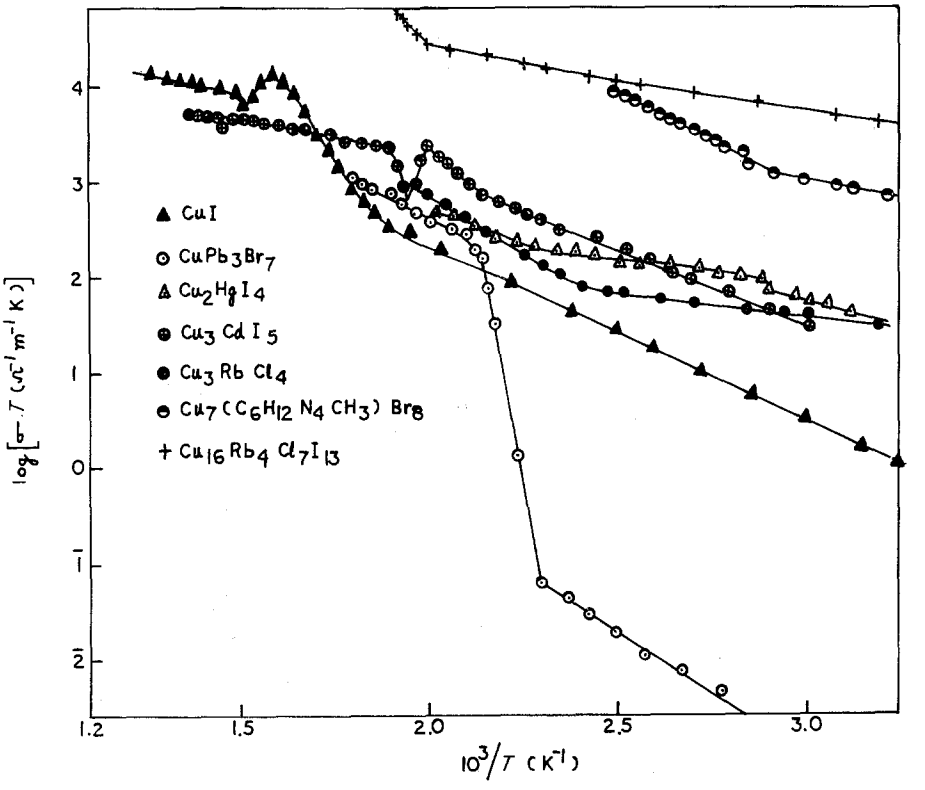

Figure 5 Plots of logarithm of the product of electrical conductivity and absolute temperature ($\log \sigma T$) against inverse of absolute temperature (T^{-1}) for the superionic solids studied.

power has also been reported. Table IV shows some common results for comparison. It is seen from this table that the order of conductivity for many of the materials reported by different workers agrees fairly well with our values. However, the magnitude of conductivity differs. This variation seems to be due to different conditions, e.g. pelletizing pressure, electrode material etc., employed by different workers. These results show that copper electroyte-based superionic solids are

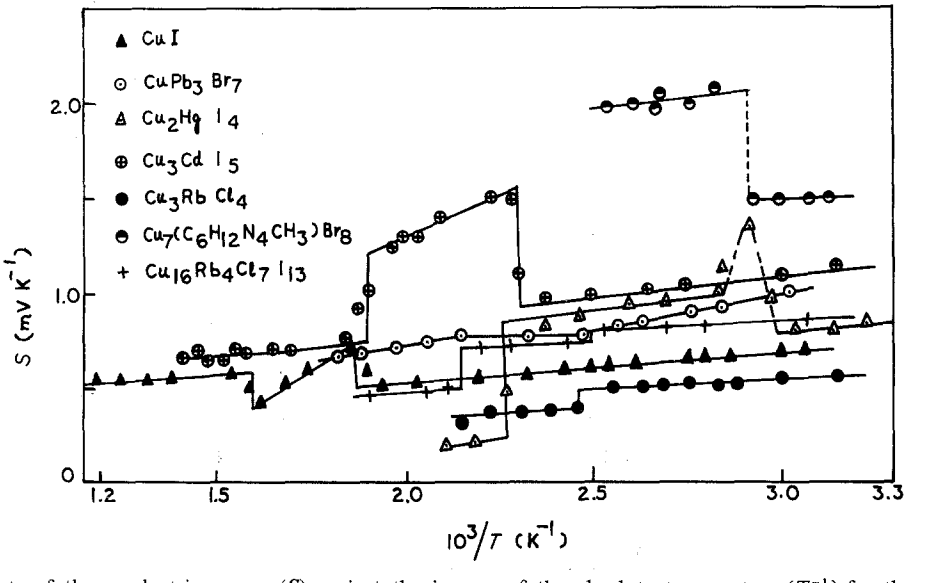

Figure 6 Plots of thermoelectric power (S) against the inverse of the absolute temperature (T^{-1}) for the superionic solids studied.

TABLE II Summarized results of thermoelectric power variation with temperature for solids studied [general expression $S = -Q/e\,(1/T) + H$]

Compound	Q (eV)	$-H$ (mV)	T^* (K)	T_B† (K)	Phase
CuI	0.20	0.11	350–525	525	N
	0.85	0.89	525–630	630	N
	0.096	0.42	650–825	–	S
$CuPb_3Br_7$	0.42	−0.26	320–410	410	N
	0.00	0.775	410–475	475	N
	0.033	0.08	475–550	–	S
Cu_2HgI_4	0.27	−0.03	300–344	344	N
	0.11	0.64	344–425	–	S
Cu_3CdI_5	0.20	0.46	350–440	440	N
	0.84	0.38	440–500	510	N
	0.078	0.55	530–710	–	S
Cu_3RbCl_4	0.05	0.40	370–405	405	S
	0.10	0.09	405–450	–	S
$Cu_7(C_6H_{12}N_4CH_3)Br_8$	0.10	1.20	300–344	344	S
	0.37	1.01	344–400	–	S
$Cu_{16}Rb_4I_7Cl_{13}$	0.075	0.61	320–400	400	S
	0.13	0.41	400–475	475	S
	0.10	0.27	475–520	–	S

*Temperature span of the linear region.
†Break temperature.

TABLE III Summarized results of electrical conductivity variation with temperature for the solids studied [general variation $\sigma T = C \exp(-E_a/kT)$]

Compound	C (Ω^{-1} m^{-1} K)	E_a (eV)	T^* (K)	T_B† (K)	Phase
CuI	1.26×10^6	0.37	350–520	520	N
	6.80×10^{11}	0.96	520–624	624	N
	1.65×10^5	0.17	660–800	–	S
$CuPb_3Br_7$	1.32×10^4	0.48	320–430	430	N
	2.56×10^6	0.37	475–555	475	S
Cu_2HgI_4	9.70×10^5	0.28	300–344	344	N
	2.19×10^3	0.11	344–425	425	S
	8.87×10^5	0.16	425–500	–	S
Cu_3CdI_5	1.63×10^6	0.31	350–470	470	N
	7.09×10^{11}	0.84	470–500	500	N
	6.42×10^4	0.15	530–730	–	S
Cu_3RbCl_4	1.25×10^3	0.10	300–420	420	S
	1.38×10^8	0.52	420–500	–	S
$Cu_{17}(C_6H_{12}N_4CH_3)Br_8$	3.75×10^5	0.16	300–344	344	S
	3.38×10^7	0.42	344–400	–	S
$Cu_{16}Rb_4I_7Cl_{13}$	3.63×10^5	0.12	310–400	400	S
	1.16×10^6	0.16	400–503	503	S

T^*, temperature span of linear region.
T_B, break temperature; N, normal; S, superionic.

TABLE IV Comparison of data in the superionic phase for the compounds investigated in present and previous studies

Compound	σ^* (Ω^{-1} m^{-1})	T (K)	E_a (eV)	Q (eV)	Reference
CuI	30	723	0.26	–	[15]
	12	723	0.19	0.098	[22]
	15	723	0.17	0.096	[PS]
$CuPb_3Br_7$	3.5	500	0.29	–	[6]
	1.3	500	0.37	0.33	[PS]
Cu_2HgI_4	1.2×10^{-3}	350	0.62	–	[14]
	5.6×10^{-4}	350	0.49	–	[2]
	2.8×10^{-1}	350	0.11	0.11	[PS]
Cu_3CdI_5	5.8	600	0.15	0.078	[PS]
Cu_3RbCl_4	0.225	298	0.18	–	[9]
	0.115	300	0.10	0.05	[PS]
$Cu_7(C_6H_{12}N_4CH_3)Br_8$	2.0	300	0.22	–	[1]
	1.9	300	0.16	0.10	[PS]
$Cu_{16}Rb_4I_7Cl_{13}$	34	298	0.10	–	[12]
	15	300	0.12	0.11	[PS]

*Values have been corrected for temperature T(K) from $\log \sigma$ against T^{-1} or $\log \sigma T$ against T^{-1} plots.

more sensitive to the method of preparation, shelf life and environmental conditions. Copper mercuric iodide is an exception in which our value is larger by two orders of magnitude and lies close to the value for a superionic conductor. A value of $0.16\,\Omega^{-1}$ m^{-1} at 333 K has been quoted [21] for Ag_2HgI_4. Both Ag_2HgI_4 and Cu_2HgI_4 have similar structures [23, 24] and we expect their σ values to be of the same order. Our values, being of the order reported for Ag_2HgI_4, seem more reliable. Furthermore, both activation energy and heat of transport for this material have been found to be equal to 0.11 eV, which indicates that this is a typical superionic conductor at $T > 344$ K.

The reported data on σ and S for the materials studied can be conventionally divided into two parts: one corresponding to the superionic phase and the other for the normal phase. It is convenient and more relevant to discuss results separately in the two phases.

4.1. Electrical transport in superionic phase

It has been established by earlier workers [1–12] that in all these solids the copper ion is the sole entity of charge carrier in the superionic phase. The movement of the ion is facilitated by its typical structure. The expressions for σ and S for the superionic phase where only one type of ion is the mobile charge carrier, have been obtained by Shahi *et al.* [20] extending the theory to normal ionic solids. Furthermore, various models have been proposed for explaining the electrical conduction in superionic conductors. Important among these models are free ion [25], lattice gas [26], ionic polaron [27] and extended lattice gas [28]. Out of these, the extended lattice gas model takes the merits of all other models and is preferred to explain our data. In this model the activation energy (E_a) and heat of transport (Q) are related by the equation [28]

$$E_a = Q + E'_a \tag{3}$$

where

$$E'_a = \frac{q^2}{4\pi^2 a \epsilon_0}\left(\frac{1}{\kappa_\infty} - \frac{1}{\kappa_0}\right) \tag{4}$$

where $E'_a = E_B/2$, E_B is the polaron binding energy, q is the charge of the mobile ion, a is their average separation, ϵ_0 the permittivity constant, and κ_∞, κ_0 are optical and static dielectric constants, respectively. Thus this model predicts the magnitude of E_a to be larger than Q. This has been found experimentally true for all solids studied except Cu_2HI_4. Thus the extended lattice gas model seems to describe the situation in all solids fairly well. Fur CuI, $\kappa_\infty = 10$, $\kappa_0 \sim 100$ and $a = 59.6$ nm. This gives $E'_a = 0.069$ eV using Equation 4, which predicts the difference between E_a and Q to be 0.069 eV. This is very close to the value of 0.074 eV found by us. The difference

TABLE V Activation energy (E_a), heat of transport (Q) and their difference for the solids studied in the superionic phase

Compound	E_a (eV)	Q (eV)	$(E_a - Q)$ (eV)
CuI	0.17	0.096	0.074
$CuPb_3Br_7$	0.37	0.33	0.04
Cu_2HgI_4	0.11	0.11	0.00
Cu_3CdI_5	0.15	0.078	0.072
Cu_3RbCl_4	0.10	0.05	0.05
$Cu_7(C_6H_{12}N_4CH_3)Br_8$	0.16	0.10	0.06
$Cu_{16}Rb_4I_7Cl_{13}$	0.12	0.075	0.045

between E_a and Q for other solids is small (Table V) which indicates that in many of the superionic solids, a static potential barrier contributes in part to the activation energy in a more significant way than caused by the dynamic process of polarization.

It is seen from Figs. 5 and 6 that even in the superionic phase the $\log \sigma T$ and S against T^{-1} slopes change greatly below their melting points. This change does not occur due to chemical instability or decomposition of the compound, because on cooling, all compounds yield nearly the same values of σ and S at room temperature. We propose that this break is due to the mobility of other cations e.g. Rb^+ in Cu_3RbCl_4 and $Cu_{16}Rb_4I_7Cl_{13}$, Hg^{2+} in Cu_2HgI_4, Pb^{2+} in $CuPb_3Br_7$ and Cd^{2+} in Cu_3CdI_5 with CuI and $Cu_7(C_6H_{12}NCH_3)Br_8$ as exceptions. All these cations, in principle, can jump from one site to another and may contribute to conductivity. This does not happen at lower temperatures because the activation energy involved in mobility is large compared to that of the Cu^+ ion. The large value of activation energy for these ions can be understood in terms of their large ionic radius (r) and charge. The ions Rb^+ ($r = 14.8$ nm), Hg^{2+} ($r = 11.0$ nm), Pb^{2+} ($r = 12.1$ nm) and Cd^{2+} ($r = 9.7$ nm) all have a bigger ionic radius than that of Cu^+ ($r = 9.6$ nm). The latter three also have twice the positive charge on them compared to the Cu^+ ion which results in a larger coloumb repulsion in their motion and thus a larger activation energy. Owing to the larger activiation energy, these ions have a negligible contribution to σ at the lower limit of the superionic phase, but their contribution increases at a much faster rate and it catches up the contribution of the Cu^+ ion at higher temperatures and gives rise to a break. The contribution of these extra cations becomes more significant where the overall conductivity due to the Cu^+ ion is comparatively small (e.g. in Cu_3RbCl_4). In $CuPb_3Br_7$, it is not apparent, because the Cu^+ ion activation energy is large and the contribution of Pb^{2+} does not get a chance to catch it up. The case for the contribution of Cd^{2+} ion in Cu_3CdI_5 is probably similar. The phase transition temperature reported here agrees fairly well with that obtained by other workers.

4.2. Electrical transport in the normal phase

Below the phase transition temperature all these solids are in a phase in which all the ions occupy specific positions. Thus β-CuI has a typical zinc blende structure, and β-Cu_2HgI_4 that of a fcc cation lattice. In general, they are similar to a normal ionic solid. Thus electrical conduction in this phase can be discussed using theories for normal solids which have been dealt with in length by many workers [29, 30]. The electrical conduction in ionic solids mainly occurs due to the motion of defects. The principal types of defect are Frenkel and Schottky defects. It is difficult to analyse data if more than one type of defect is present. The superionic solids have a cationically disordered lattice in the superionic phase. In the lower temperature phase, the cationic disordering tendency is more natural in such solids. Formation of Frenkel defects has been accepted [21] in almost all types of Ag^+ ion conducting superionic solids. The copper ions with smaller ionic radi compared to silver ($r = 11.3$ nm), can more easily stabilize themselves in interstitial positions. Thus we shall attempt to explain our data on the assumption that Frenkel defects are more mobile in these solids.

When the temperature of the material is not very high, the number of defects are usually constant over a fairly wide range of temperature, in such a situation the variation of σT with T is given [21] by the equation

$$\sigma T = C_1 \exp\left(-\frac{h_f}{kT}\right) \tag{5}$$

where C_1 is nearly constant and h_f is the enthalpy for the migration of mobile defects. However, at a sufficiently high temperature, thermal energy begins to generate defects and the expression for σT becomes [21, 28, 29]

$$\sigma T = C_2 \exp\left(\frac{H_f + 2h_f}{2kT}\right) \tag{6}$$

where C_2 is a constant and H_f is the enthalpy of formation of the Frenkel defect. Both Equations 5 and 6 predict linear $\log \sigma T$ against T^{-1} plots with a change in slope at some temperature, T_k, usually referred as the Knee temperature. The higher temperature region (usually referred as the intrinsic region) is associated with a higher slope $[E_a = (H_f/2) + h_f]$ and the lower temperature region (referred as the extrinsic region) with a lower slope $(E_a = h_f)$. Similarly, the expression for S where only Frenkel defects are mobile is given by the expression [16, 21]

$$S = -\frac{Q}{eT} + \frac{1}{e}\left[k \log\left(\frac{n}{N}\right) + \frac{\partial g}{dT} - S\right] \quad (7)$$

where Q is the heat of transport for the mobile species, n and N are the number of defects and normal sites per unit volume, respectively, g is the amount of work required to bring the cation (Cu^+ ion in present case) from a state of rest at infinity to an interstitial position in the solid at constant temperature and pressure, and S is the partial entropy of the Cu^+ ion in copper metal. The number, n, at any temperature can be expressed by the relation [21]

$$n = (NN')^{1/2} \exp(-H_f/2kT) \quad (8)$$

where N' is number of interstitial sites per unit volume available for the Cu^+ ion. Since N and N' are nearly the same, one can write from the above equation

$$\frac{k}{e} \log\left(\frac{n}{N}\right) = -H_f/2eT \quad (9)$$

Normally the sum of the third and fourth terms of Equation 7, becomes nearly temperature independent, as variation of one nearly compensates the other [21], and we can express this by the temperature independent constant, S_1. Thus from Equations 7 and 9, we can write

$$S = -\frac{1}{eT}\left(Q + \frac{H_f}{2}\right) + S_1 \quad (10)$$

Obviously this refers to the intrinsic region. In the extrinsic region, n is practically constant and then the expression for S reduces to

$$S = -\frac{Q}{eT} + H \quad (11)$$

where H is now independent of T. Thus a plot of S against T^{-1} should be a straight line with a break in the slope at the Knee temperature. The higher temperature region should give an apparent value of $Q_a = Q + H_f/2$ and a lower temperature equal to Q.

In the light of the above discussion, we can analyse the experimental data in the normal phase and obtain values of Q, H_f and h_f. The phase transition temperature of Cu_3PbCl_4, $Cu_7(C_6H_{12}N_4CH_3)Br_8$ and $Cu_{16}Rb_4I_7Cl_{13}$ lies below room temperature and since our studies are above this temperature, we have not observed the normal phase for these materials.

For CuI and Cu_3CdI_5, we obtained two distinct regions and from these we obtained values of h_f, Q and H_f. H_f was evaluated from both σ and S data and the values differ little, as is evident from Table VI. This justifies the validity of the proposed conduction mechanism. For $CuPb_3Br_7$, the $\log \sigma T$ as well as S against T^{-1} plots have two distinct regions. But here the S plot for the upper region has an almost zero slope. We expect a much higher slope for the intrinsic region. Thus nearly linear $\log \sigma T$ against T^{-1} plots on the higher side of T do not represent the intrinsic region. In fact, the temperature is too low for the appearance of the intrinsic region.

For Cu_2HgI_4, the phase transition temperature is 344 K; below this temperature we obtain linear $\log \sigma T$ and S against T^{-1} plots. It refers to an extrinsic region because it has a lower value of slope and we do not expect the appearance of an intrinsic region at such a low temperature. The calculated values of E_a and Q for $CuPb_3Br_7$ and Cu_2HgI_4 from the lower temperature region slope, thus give the value of energy for the

TABLE VI Values of h_f, Q and H_f as deduced by σ and S in the normal phase of the solids studied

Compounds	σ_{meas}			S_{meas}		
	$H_f/2 + h_t$ (eV)	h_f (eV)	H_f (eV)	$Q + H_f/2$ (eV)	Q (eV)	H_f (eV)
CuI	0.96	0.37	1.18	0.85	0.20	1.30
$CuPb_3Br_7$	–	0.48	–	–	0.42	–
Cu_2HgI_4	–	0.28	–	–	0.27	–
Cu_3CdI_5	0.84	0.31	1.06	0.84	0.20	1.28

migration of defects (h_f) and the heat of transport for the defect, respectively.

Acknowledgement

Part of this work was supported financially by CSIR, India and the authors acknowledge it with thanks.

References

1. T. TAKAHASHI, S. IKEDA and O. YAMAMOTO, *J. Electrochem. Soc.* **120** (1973) 647.
2. S. SHIBATA, H. HOSHINO and M. SHIMOJI, *J. Chem. Soc. (Faraday Trans. I)* 70 (1974) 1409.
3. T. TAKAHASHI and O. YAMAMOTO, *J. Electrochem. Soc.* **122** (1975) 83.
4. A. F. SAMMELLS, J. G. GOUGOUTAS and B. B. OWENS, *ibid.* **122** (1975) 1291.
5. T. TAKAHASHI, O. YAMAMOTO, F. MATSUYAMA and Y. NODA, *J. Solid State Chem.* **16** (1976) 35.
6. T. TAKAHASHI, Y. YAMAMOTO and H. TAKAHASHI, *ibid.* **21** (1977) 37.
7. M. LAZZARI, S. SCROSATI and C. A. VINCENT, *Electrochimia Acta* **22** (1977) 51.
8. V. V. ALPEN, J. PENNER, J. D. MARCOLL and A. RABENAU, *ibid.* **22** (1977) 81.
9. J. MATSUI and J. B. WAGNER Jr, *J. Electrochem. Soc.* **124** (1977) 941.
10. T. TAKAHASHI, O. YAMAMOTO and A. SAWAI, *J. Appl. Electrochem.* 8 (1978) 161.
11. R. H. DAHM, S. HACKWOOD, R. G. LINFORD and J. M. POLLOCK, *Nature* **272** (1978) 522.
12. T. TAKAHASHI, O. YAMAMOTO, S. YAMADA and S. MAYASHI, *J. Electrochem. Soc.* **126** (1979) 1684.
13. S. CHANDRA, "Superionic solids: Principle and application" (North Holland, Amsterdam, 1981) and references therein.
14. L. SUCHOW and G. R. POND, *J. Amer. Chem. Soc.* 75 (1953) 524.
15. W. BIERMANN and H. J. OEL, *Z. Phys. Chem.* **17** (1958) 163.
16. B. K. VERMA, O. P. SRIVASTAVA and H. B. LAL, *Phys. Status Solidi (a)* **64** (1981) 467.
17. O. P. SRIVASTAVA, PhD thesis, Gorakhpur University, Gorakhpur, India (1983).
18. H. B. LAL and O. P. SRIVASTAVA, *Phys. Status Solidi (a)* 77 (1983) 405.
19. *Idem, J. Mater. Sci.* 19 (1984) 303.
20. K. SHAHI, H. B. LAL and S. CHANDRA, *Ind. J. Pure Appl. Phys.* **13** (1975) 1.
21. K. SHAHI, *Phys. Status Solidi (a)* 41 (1977) 11.
22. B. K. VERMA, V. PRATAP and H. B. LAL, *Jpn. J. Appl. Phys.* 20 (1981) 467.
23. J. A. A. KETELAAR, *Z. Krist.* (*A*) 87 (1934) 436.
24. S. M. GIRVIN and G. D. MAHAN, *J. Solid State Chem.* **23** (1977) 629.
25. M. J. RICE and W. L. ROTH, *ibid.* 4 (1972) 294.
26. W. J. PARDEE and G. D. MAHAN, *ibid.* 15 (1975) 310.
27. C. P. FLYNN, "Point defect and diffusion" (Oxford University Press, London, 1972).
28. G. D. MAHNN, *Phys. Rev.* **B14** (1976) 780.
29. A. B. LIDIARD, in "Handbuch der Physik", Vol. 20, edited by S. Flugge (Springer Verlag, Berlin, 1957) p. 246.
30. P. SUPTITIZ and J. TELTOV, *Phys. Status Solidi* 23 (1967) 9.

Received 24 November 1983
and accepted 11 July 1984